JOINT EUROPEAN TORUS

JET–P(88)52

D.J. Gambier, M.P. Evrard, J. Adam, A. Becoulet , S. Corti, P. Hennequin,
J. Jacquinot, D.F.H. Start, K. Thomsen, B.J.D. Tubbing, V. Zanza
and JET Team

ICRF Power Deposition Profile and Determination of χ_e by Modulation Experiments in JET

ICRF Power Deposition Profile and Determination of χ_e by Modulation Experiments in JET

D.J. Gambier[1], M.P. Evrard[2], J. Adam[1], A. Becoulet[1], S. Corti, P. Hennequin[3], J. Jacquinot, D.F.H. Start, K. Thomsen, B.J.D. Tubbing, V. Zanza and JET Team*

JET-Joint Undertaking, Culham Science Centre, OX14 3DB, Abingdon, UK

[1]Association EUR-CEA, CEN Cadarache, France
[2]ERM/KMS Brussels, Belgium
[3]Laboratoire P.M.I., Ecole Polytechnique, Palaiseau, France
[4]ENEA Frascati, Italy
** See annex of P. Lallia et al, "Plasma Heating in JET",*
(13th EPS Conference on Controlled Fusion and Plasma Physics, Schliersee, Germany (1986)).

Preprint of Paper to be submitted for publication in
Nuclear Fusion

ABSTRACT.

The question of ICRF power deposition profile in JET is experimentally addressed by means of a square wave modulated RF perturbation. The study is conducted in D(H) and D(He^3) plasmas for two heating scenarios.

In D(He^3) plasmas and for central heating in a scenario where mode conversion into a Bernstein wave is accessible, the direct power deposition profile on electrons is derived. It accounts for 15% of the total coupled power and extends over 25% of the minor radius.

Outside the RF power deposition zone, observation of the diffusive electronic transport enables an estimation for χe inside the inversion radius surface (r_i). In non monster-sawtooth discharges and for low central temperature gradient ($\nabla T_e(r \leq r_i) \leq \nabla T_e(r \geq r_i) \approx 5$ keV/m), the obtained value is small ($\approx 0.24 \pm 0.05$ m^2/s), typically a tenfold lower than estimations of χe deduced by heat pulse propagation on similar discharges at radii larger than the inversion radius.

In D(H) and for the minority heating scheme, a large fraction of the ICRF modulated power is absorbed by the minority ions and modulation of the minority tail is observed with a characteristic i-e slowing down time. In this scheme, electron heating occurs only through collisions with the minority ion tail and the modulation of the electron temperature is unobservable in sawtoothing discharges. This is interpreted as a consequence of the long i-e equipartition time, acting as an integrator for the modulated ICRF signal.

Finally, a correlation between the time of the sawtooth crash and the periodic turn off of the ICRF power is evidenced and its consequence for modulation experiment is reviewed.

I. INTRODUCTION.

In tokamaks, the determination of ICRF power deposition profiles allows to address the question of the overall power balance of the discharge during auxiliary heating [1]. The ICRF modulation technique provides a means to derive the mechanism of ICRF power transfer to species and to measure the ICRF power deposition profile.

The Ion Cyclotron Frequency wavelength being of decimeter order ($\lambda \approx C_A/\nu_{RF}$, where C_A is the Alfven velocity and ν_{RF} ranges from 20 to 120 MHz), it was also, in the generation of tokamaks prior to JET, of order of the minor radius and the wave pattern was mainly dominated by diffraction and not by the particle absorption. Thus diffraction prevented from measuring the power deposition profile. Only in PLT (minor radius 40 cm) was this measurement attempted, taking advantage of a well adapted charge exchange diagnostic with angles of observation varying from approximately perpendicular to parallel [2]. The net result, when simulated with a bounce averaged Fokker Planck code, shows that the power deposition profile is broad. In JET the wavelength limitation no longer holds and a study of the shaping of the ICRF power deposition profile can be undertaken.

The ICRF heating scheme relies on the absorption of a Fast Magnetosonic Wave (FMW). It can be directly absorbed by ions ($\omega=\omega_{ci}$, $\omega=2\omega_{ci}$) or by electrons through Landau damping at high temperatures, or be mode converted on a slow wave of decreasing wavelength, which in contrast can be absorbed by electrons through parallel Landau damping. The heating deposition profile is then localized around the cyclotron resonance for ions and around the mode conversion layer for electrons. In the present experiments three antennae were installed on the outer side of the torus [3], and the heating scheme was either Hydrogen or Helium 3 minority in Deuterium plasmas.

A first attempt to obtain the power deposition profile used the slope of the electron temperature after each sawtooth crash [4] at different radii in order to derive locally the amount of power coupled to electrons. In so doing a fraction of the measured power is coming from the ohmic heating power and must be subtracted. This is achieved by measuring the slope of the sawtooth during the ohmic phase only and correcting for variations in temperature and density during the RF phase. However, this procedure is unsatisfactory for it implicitly assumes that characteristics of the target plasma have remained unchanged during both phases (as for example the radiative power and the confinement properties).

Ideally, a figure for the power amplitude is achieved when the time response to the perturbation is adiabatic. This ensures that the measurement of the $T_e(t)$ derivative, when convoluted with the density variation, is a direct measurement of the ICRF power absorbed by

electrons. Indeed, this method has been widely used at the onset of the RF power. However the accuracy is limited by the imprecision of $dT_e(t)/dt$ measurements.

The power amplitude modulation technique generalizes the two previous approaches. The JET RF generators have a switch-on time in the msec range, so that the RF power can be square wave modulated and the long plasma discharge sustained in JET ($\leq$15 sec) allows extensive use of noise rejection techniques. The present analysis is conducted mainly using Fourier transformed signals with emphasis on Fourier components at the fundamental modulation frequency $\tilde{\omega}$. However "box car" integration is also used to compute the electron temperature response to the imposed square wave power modulation.

The present article is organized as follows: in the next section, the experimental arrangement is presented. In §III, the time response of $T_e(t)$ to a sinusoidal and a square perturbation function is modelled in order to appreciate the effect of diffusion and confinement. Results of modulation in D(H) plasmas are analyzed in §IV and effects of large sawtooth crashes on Fourier components are reviewed. While no T_e modulation is retrieved, the net result comes from charge exchange analyzers, giving an estimation for the slowing down time of the fast ions at different energies. In section VI, direct electron heating is demonstrated in the $D(He^3)$ scheme and the power deposition profile is deduced. Furthermore as a result of modulation experiments, an estimation for χ_e in the plasma central region may be obtained showing that the confinement is, in this case, better in the central region than in the gradient zone. This method appears complementary to the derivation of χ_e by heat pulse propagation studies in the gradient zone [5].

II. EXPERIMENTAL SET UP AND DATA ANALYSIS.

The electron temperature is measured on JET by three different Electron Cyclotron Emission (ECE) diagnostics: a Michelson interferometer which is absolutely calibrated [6] and serves as a reference for other diagnostics, a Fabry-Perrot and a grating polychromator. The polychromator [7], based on detection of the electron cyclotron second harmonic emission in the extraordinary mode for which the optical depth is large, monitors the electron temperature at 12 different radii and is well suited for profile analysis. To avoid superposition of modes, temperatures are only monitored on the low magnetic field side of the plasma. The absolute calibration error is estimated to be 5% while the error on the radial position varies between 11 cm in the plasma center to 5 cm at radii larger than 30 cm. In the reported experiments, the data acquisition sampling time for the RF and temperature signals was set to 500 μs or 624 μs and each signal recorded in a 16 k-octet memory.

For typical JET discharges reported therein, the sawtoothing activity is large and may conceal any modulation observation. To ease the separation between sawtooth and

modulation, a preprocessing of the $T_e(t)$ signal has been devised to suppress sawtooth crashes. The $T_e(t)$ signal is digitally separated into a Linear Sawtooth Signal (LSS) and a Modulated Temperature Signal (MTS). To construct the LSS the occurrence of sawtooth crashes are detected, as well as T_e values before and after the crash. A linear sawtooth is then reconstructed by linear interpolation between the bottom value of T_e at the crash and the top value at the next crash. The MTS is eventually computed as the residual signal when the LSS is subtracted from the raw data. Although the sawtooth crash is not completely suppressed from the MTS, it is nevertheless substantially removed : from 1-2 keV in the $T_e(t)$ signal, the residual sawtooth crash is only 50 eV or less. A drawback of the algorithm effectiveness is its crucial dependance upon the sawtooth crash detection. Outside the inversion radius, sawtooth crashes are mixed with partial sawteeth and postcursors which, when added to the adverse effect of the dilution of RF power in a larger volume, explains why to date no off axis heating modulation experiment has been successfully analyzed.

Each signal (MTS or LSS) can be analyzed using either the "boxcar" technique ($S_B(t) = \frac{1}{N+1} \sum_{k=0}^{N} S(t + kT)$; $t \in [0,T]$) [8] or the Fast Fourier Transform (FFT). In the case of the FFT, the coherence of the measured $\overline{T}_e(\tilde{\omega})$ can be evaluated in one shot, allowing for an underestimation of the error $\delta\overline{T}_e(\tilde{\omega})$ [9].

III. ANALYSIS OF THE MODULATED POWER BALANCE EQUATION.

For a given species, the power balance equation accounts for the competition between power source and loss terms. The different processes of heat transfer involved are : equipartition of energy between species, heat conduction and convection, radiation and charge exchange losses, power sources (ohmic and ICRF). To understand what may be gained in Fourier analyzing the response signals a simple linear model is constructed for the electron power balance.

In this model, convection and variation in density profile are neglected to write the electron power balance equation as :

$$\frac{\partial}{\partial t} W_e(r,t) = \frac{2}{3}\chi_e \Delta W_e(r,t) - \frac{W_e(r,t)}{\tau_*} + P_e(r,t), \qquad (1)$$

where power losses are represented by the electron thermal diffusivity χ_e (fixed in this model; $\chi_e(r,t) = cst.$) and by the phenomenological second RHS term. The latter includes all other non transport mechanisms of loss experienced by the species and $P_e(r,t)$ is the sum of the ohmic and RF power. The RF power itself contains two terms : the direct RF heating power which occurs

through direct Landau absorption, TTMP or Landau absorption of mode converted waves and the indirect heating through Coulomb collisions with the high energy tail developed by the minority ion species.

In the Fourier analysis, we focus on the linear modulated electron response to the ICRF power varying as : $\tilde{P}_{RF}(\mathbf{r},\omega,t) = \tilde{P}_{RF}(\mathbf{r},\omega)\, e^{i\omega t}$. In particular, at first order in $e^{i\omega t}$, the modulated ohmic power is neglected as small compare to the RF power. For sake of clarity, a 1-D model is considered with direct RF heating ($\tilde{P}_{RF}(x,\omega) = \tilde{P}_{RF}(x)$). Then the electron response may be written in terms of a Green function :

$$\tilde{W}_e(x,\omega,t) = e^{i\omega t} \int_{-\infty}^{+\infty} G(x-\zeta,\omega).\tilde{P}_{RF}(\zeta).d\zeta \,, \qquad (2\text{-a})$$

where the Green function is expressed as:

$$G(x-\zeta,\omega) = \frac{\tau^*}{1+i\omega\tau^*}\frac{k}{2}\, e^{-k|x-\zeta|} \quad (2\text{-b}) \quad \text{and} \quad k^2 = \frac{1+i\omega\tau^*}{\frac{2}{3}\chi_e\tau^*} \,.$$

In the high frequency limit ($\omega\to\infty$) the expression $\frac{k}{2}e^{-k|x-\zeta|}$ tends towards $\delta(x-\zeta)$ and the derivative of the modulated response matches the ICRF power deposition profile $\tilde{P}_{RF}(x)$ as already noticed in [10].

In the case $\omega\tau^* \gg 1$, the response is only affected by the diffusivity χ_e. This effect is illustrated in Fig.1-a for $\tilde{W}_e(x,\omega)$ and a square deposition profile of width Δ. Inside the domain of the deposition profile the phase shift of the response with respect to the driving power is mainly constant and the amplitude slowly decreases. Although the Full Width at Half Maximum of the amplitude is indicative of the power deposition profile extension, it should be noticed that : when Δ is less than the FWHM Δ' of the Green function ($\Delta' = \ln(4)/\sqrt{3\omega/4\chi_e}$), then a constant phase evolution is a better indicator of the profile extension. The overall phase lag introduced by the Green function (eq.2-b) is bounded by $\pi/4$ and 0 depending upon the width of the deposition profile ($\pi/4$ corresponds to $\tilde{P}_{RF}(x) = \delta(x)$ and 0 to $\Delta\to\infty$, while $\pi/4$ comes from the 1-D model, in 2-D it becomes $\pi/8$ and 0 in 3-D).

Outside the Δ domain, diffusion dominates the phase variation with x, at a rate :

$$k_D = \frac{\delta\Phi}{\delta x} = \sqrt{\frac{3\omega}{4\chi_e}}, \qquad (3)$$

which allows a determination of χ_e. The propagation of heat is governed by the wave vector k_D, independent of the model dimensionality, and the amplitude decreases as $e^{-k_D x}$ (Fig. 1-b). In practice, the measurement of k_D relies on the phase of the Fourier component $\overline{T}_e(x,\omega)$ and gives an averaged value of χ_e over the RF pulse length. However, eq.1 does not contain any transient phenomena such as the sawtooth crashes, which may be misleading (cf.§.IV). Therefore in the Fourier analysis of experimental signal, a figure for χ_e may only be derived from the MTS signal, where sawtooth crashes are partially eliminated.

To escape from such potential prejudice in χ_e measurements, it is possible to take advantage of the adiabatic plasma response to a square modulated pulse. Indeed at each periodic onset (offset) of the RF power, the electron temperature slope changes and generally occurs at time different from the sawtooth crashes. Due to diffusion, the time at which the slope is changing increases with increasing distance from the heating zone. A 1-D model, based upon the previous formalism but for a square hat waveform, allows the time delay to be obtained when the χ_e value is imposed. Inside the power deposition zone, the slope of $\tilde{T}_e(x,t)$ responds with no time delay, while outside the response suffers a longer delay at larger radii. A significant shift is revealed (Fig.2) for the JET parameters reported hereafter only if χ_e is small, typically $\chi_e \approx 0.25$ m^2/s.

The case of indirect electron heating raises further questions and has been addressed in a companion paper [11] where it is shown that : in the absorption of the ICRF power by minority ions, an energetic tail develops and the high energy part of the tail responds linearly to the modulation, if the averaged ICRF power is large compared to the modulation amplitude. Furthermore for high ICRF power density [12], the dominant Coulomb collisions of minority ions are with electrons. The power deposition profile on electrons reduces to:

$$\tilde{P}_{RF}(r,\omega) = \frac{1}{1+i\omega\tau_S} \int_{-\infty}^{+\infty} G(r-\xi,\omega)\tilde{P}_{RF}^{min}(\xi)\, d\xi ,$$

where minority ions integrate the modulated ICRF power. The power amplitude deposited on electrons is reduced by $1/\omega\tau_S$, where τ_S is the relaxation time of the minority tail. For the case considered in this article τ_S reaches 0.11 s in D(H_e^3) plasmas and 0.16 s in D(H) [13] and the net reduction ranges from 5 to 10, a figure prejudicial to the method.

IV. ICRF MODULATION IN D(H) PLASMAS : CORRELATION WITH SAWTOOTHING ACTIVITY.

A series of experiments were conducted in D(H) plasmas with main parameters listed in table I. The ICRF and the modulation frequencies were set to 47.7 MHz and 12.5 Hz respectively. The coupled power amplitude of 1.3 MW was modulated in square wave while the antenna was operating in the monopole mode. The radii of observation ranged from 2.97 to 3.61 m allowing for an observation mainly in the plasma center.

Table I : D(H) plasma parameters.

$B_T = 3.4$ T	$I_P = 2.8$ MA	$T_{e0}(\Omega) = 3.3$ keV	$T_{i0}(\Omega) = 2.3$ keV	$n_{e0}(\Omega) = 3.4\ 10^{19}$ m^{-3}
$Z_{eff} = 2.1$	$n_H/n_D = 3\%$	$q_C = 4$, $q_\psi = 6$	$R_{cH} = 3.29$ m	$R_0 = 3.04$m, $R_i = 3.45$m

The minority Hydrogen tail is monitored by the neutral particle analyzer. A set of five analyzers scan the plasma cross section [11]. Only channels viewing the plasma center exhibit an increase in neutral fluxes (Fig.3), showing a centrally peaked power deposition profile on minority ions. From raw data, sawtooth crashes are on average small compared to the modulation amplitude and therefore not prejudicial to the analysis. The "box car" responses to the RF modulation (Fig.4 for two neutral particle energies 10 keV and 70 keV) exhibit the main following features : the low energy channel responds to the modulated power on a time scale of the order of 10 ms and then saturates; the high energy channel on the contrary, is not yet saturated at the end of the half modulated period. This demonstrates that the time for the high energy part of the tail to reach saturation is much longer than 40 ms. Those observations are in relative agreement with predictions for equipartition times. At low energy protons mainly collide with background Deuterium ions and the relaxation time [14] is 11 ms in good agreement with the observed value. At high energy the fast protons collide mainly with electrons and the relaxation time for energy transfer reaches 150 ms, while the slowing down time of the overall distribution function establishes itself at 147 ms [13], which is not contradicted by the experimental value.

If we now focus on electrons, we first observe that during the RF modulation pulse the central density rises steadily (Fig.5). This indicates that the modulation of the density in the electron power balance does not need be considered at that location. When the RF is switched on, the electron temperature at all radii only responds to the averaged ICRF power as illustrated in Fig.6 by the slow rise of the electron temperature slope over 300 ms. This observation is

further confirmed in the Fourier MTS spectrum (Fig.7-a) where no clear peak can be discerned from the noise at the modulation frequency.

The Fourier LSS spectrum $\overline{S}_r(\omega)$ presents (Fig.7-b) a maximum reaching 200-300eV at the quasi sawtooth frequency of 4-8 Hz and a narrow and large peak at the modulation frequency : $\overline{S}_r(\tilde{\omega}) \approx 150$ eV. A correlation then exists between the noise (i.e. the sawteeth) and the modulated RF signal. The histogram of the sawtooth crashes related to the modulation period (Fig.8) allows to estimate the standard deviation σ as :

$$\sigma = \frac{1}{\sqrt{N}} |N_+ - N_-|,$$

where N is the total number of crashes during the RF pulse, N_+ the number of crashes occurring during the RF on phase ($N = N_+ + N_-$). σ represents the number of standard deviations from a uniform distribution (for which $\sigma=0$). In the case of Fig.3, $\sigma=3.25$ and the probability for the distribution to be uniform is less than 2%.

The responsible mechanism for this correlation on the Fourier transform of $T_e(t)$ has been simulated as follows : first an artificial sawtoothing signal is constructed, with a constant slope and a random period uniformly distributed in the interval $[0.8T_{st}, 1.2T_{st}]$ with T_{st}=140 ms the averaged period (Fig.9, trace (1)). The corresponding spectrum is presented in Fig.10-a and reproduces the main features of an experimental spectrum for $\overline{T}_e(\omega)$. To simulate the correlation with the RF modulated pulse (ν = 12.5 Hz, Fig.9 trace (2)), the sawtoothing signal is modified. Crashes which were occurring during the RF on phase are delayed or advanced to fall in the nearest RF off phase, where they are randomly reallocated according to a uniform distribution (Fig.9, trace (3)). This emulates a case where the correlation is maximum ($\sigma=\sqrt{N}$). The resulting spectrum is presented in Fig.10-b. Although there is no RF heating power, a narrow peak is observed at the modulation frequency.

This simulation demonstrates the existence of a correlation between the sawtooth and the RF modulation period. Although the responsible mechanism remains conjectural, it could be proposed that the electron temperature modulation must have a counterpart in the pressure profile through the fast ion tail, which is a possible source for monster sawtooth or fish bones [15].

From the experimental observations it results that : (i) the averaged evolution of $T_e(t)$ shows qualitatively the existence of indirect electron heating, however the integrator role of the minority prevents the associated modulated electron response to be quantified; (ii) the power directly absorbed by electrons is embedded in the noise ($\Delta T_e \leq 10$ eV) for T_e in the range of 3 keV and is inaccessible to experimental measurements. Theoretical simulations using a full wave 2-D code [16] confirm those observations : for a parallel wavenumber launched by the

antenna of 4 to 7 m^{-1}, no mode conversion is predicted and all the ICRF power is absorbed by the minority ions. In conclusion, the central heating experiment tends to support the prediction that most of the RF power is absorbed by the minority Hydrogen ions.

V. MODULATION IN D(He3) : DETERMINATION OF THE ELECTRON DIFFUSION COEFFICIENT.

Modulation experiments were conducted in D(He^3) plasmas (Table II). ICRF and modulation frequencies were set to 29.9 MHz and 5 Hz respectively. The coupled power amplitude of 1.3 MW was square wave modulated. The radii of observation of the electron temperature ranged from 2.70 to 3.25 m and 3.05 to 3.60 m in two consecutive discharges allowing observation across a large part of the central plasma cross section.

Table II : D(He^3) plasma parameters, index 0 refers to the stationary ohmic and RF phase.

$B_T = 3.08$ T	$I_P = 2.7$ MA	$T_{e0} = 3.5$ keV	$T_{i0} = 2.8$ keV	$n_{e0} = 2.4\ 10^{19}$ m^{-3}
$Z_{eff} = 5.0$	n_{He3}/n_D= 15-30%	$q_C = 4$, $q_\psi = 6$	$R_{cHe3} = 3.20$ m	$R_0 = 3.13$m, $R_i = 3.48$m

In figure 11 the evolution of the main parameters is presented: (i) as in the previous case the density in the center is not modulated and rises steadily during the RF pulse, (ii) the electron temperature exhibits slope variations at the periodic RF turn on and off times (also Fig. 12-a), (iii) the temperature of Deuterium ions, monitored by the neutron emission, presents small modulations, (iv) the plasma total energy, deduced from magnetic measurements, has a 100 ms response time which prevents from observing modulation effects. Furthermore the emission from ionization states of low Z impurities is correlated with the modulated power while Z_{eff}, deduced from Bremsstrahlung, is not. No attempt has however been made to relate the modulated impurity behavior with the RF power.

During the RF on phase, the averaged slope of the electron temperature (Fig.12-b), is larger than its ohmic equivalent. When the RF power has been turned off this remains for 200-300 ms, indicating that either a minority He^3 tail has developed to energies such that collisions with electrons are effective or that the Deuterium temperature has been increased so that the equipartition between the two species relaxes on a typical equipartition time. In such conditions, the slowing down time [13] for the minority tail is 100 ms while the equipartition time with deuterium ions is 200 ms. The averaged slope of electrons at the turn off of the RF power is 5.0 keV/s compared to 2.9 in the following stationary ohmic phase, leaving 2.1 keV/s

as an heating source. Considering only the equipartition with deuterium ions, the difference of heating power available between the RF turn off and during the stationary ohmic phase is:

$$\Delta\left\{\frac{T_e - T_D}{\tau_{eq}}\right\} \approx 2.0 \text{ keV/s} .$$

where $T_{e0}(\Omega)$= 2.6 keV, $T_{i0}(\Omega)$= 2.2 keV, $n_{e0}(\Omega) = 2.2\ 10^{19}$ m^{-3} and $T_{e0}(T.O)$= 2.6 keV, $T_{i0}(T.O)$= 2.7 keV, $n_{e0}(T.O) = 2.8\ 10^{19}$ m^{-3} with the electron temperature taken at the bottom of the sawtooth. This figure is therefore not in favour of an indirect heating through the minority tail.

The change of slope at the periodic RF turn on and off time is a clear characteristic of direct RF electron heating. In those particular discharges, the amplitude of $\overline{S}\,\tilde{\omega}(r)$ is small and the histogram of sawtooth crashes indicates a σ of 0.3, showing that the distribution is almost uniform and that the amplitude of $\overline{T}_e(\tilde{\omega})$ is dominated by the linear response to the modulated RF pulse. However when observing the raw MTS signal (Fig.13), the sawtooth crashes, even largely attenuated, are still present as a residue in $\tilde{T}_e(t)$ (due to a saturation effect occurring just before the onset of the crash). As crashes occur mainly at times close to the maximum amplitude response, the effect of the residual sawtooth is : (i) to truncate the maximum $\tilde{T}_e(t)$ response and eventually to lower the amplitude of $\overline{T}_e(\tilde{\omega})$, (ii) to increase the error bar on the χ_e determination.

The power deposition profile is presented on Fig.14. From the adiabatic slope variation averaged over the number of modulated periods, the direct heating power deposition profile is measured and appears roughly square over 30±5 cm. However, the error bars on the amplitude are large due to the estimation of $T_e(t)$ time derivatives. For proper comparison, the Fourier counterpart $\tilde{\omega}\overline{W}_e(\tilde{\omega},R)$ ($\overline{W}_e(\tilde{\omega},R)=\frac{3}{2} n_e \overline{T}_e(\tilde{\omega},R)$) is multiply by $\pi/4$ to correct for the main RF power component $\overline{P}_e(\tilde{\omega})$ $4/\pi$ larger than its averaged value over time. Due to the effect of both diffusion and residual sawtoothing activity, the Fourier profile shape is smoother than its adiabatic counterpart. The central value reaches 35 kW/m^{-3} in the adiabatic case (67 kW/m^{-3} per MW of RF power) and for the Fourier counterpart 25 kW/m^{-3} (50 kW/m^{-3}/MW). The volume integrated power is then 76 and 60 KW respectively. The total power coupled to the plasma for the first harmonic of the modulation being 520 KW, the total power coupled on electrons accounts for 15%. This last figure is an estimate of the amount of mode conversion for this particular heating scheme.

For those parameters, a 2-D numerical simulation [16] shows that the amount of mode conversion is predicted to be 30% at $k_{//} = 5$ m^{-1} and $n_{He3}/n_D = 30\%$, while the FWHM for the mode converted power is 35 cm. Considering the large experimental uncertainty upon

the ratio $n_{He3}/n_D \approx$ 15-30% and the fact that both resonances are located close to the plasma center those figures appear to be in fair agreement with the experimental result. Finally the amplitude response of $\overline{T}_e(\tilde{\omega})$ vs. $\tilde{\omega}$ is plotted in Fig.15 for 3 different frequencies (5, 12.5, 25 Hz). We observe that $\overline{T}_e(\tilde{\omega})$ is proportional to $\tilde{\omega}^{-1}$ confirming the direct heating scenario.

From the phase profile, we observe that it is roughly constant over 25±5 cm, confirming the extension value of the power deposition profile. This value is much smaller than the diameter of the q=1 surface (0.70 m). Outside this domain the phase lag increases linearly with radius (Fig.16-a). Interpreting the phase lag as due to diffusion, it is found $\chi_e \approx 0.24 \pm 0.05$ m^2/s, a figure very small compared to the estimation of χ_e in the gradient zone obtained from sawtooth heat pulse propagation [5] ($\chi_e \approx$ 2-4 m^2/s).

This is further confirmed by observing the time delay vs. radius of the adiabatic response (Fig.16-b) after the onset of the RF power. The response has been averaged over the number of RF periods using the "box car" technique. For the radii analyzed (3.2 and 3.4 m), no residual sawtooth occurs during the heat propagation delay, and the interpretation in terms of a χ_e is meaningful. Inside the deposition profile the time delay is zero while outside it varies at a rate of 250 ± 50 ms/m. Interpreted in the frame of our model (cf.§III) a value of $\chi_e \approx 0.27 \pm 0.04$ m^2/s must be chosen to fit the observed delay, confirming the previous value.

Therefore in sawtoothing discharges and provided ∇T_e remains small ($\nabla T_e(r \leq r_i) \leq \nabla T_e(r \geq r_i) \approx$ 5 keV/m), the central plasma region is characterized by an improved confinement over the overall plasma. This experimental result comes as a confirmation of spectroscopic and MHD results from experiments of laser blow off impurity injection in PLT [17] where the reduction in diffusion in the plasma center was a necessary hypothesis in simulating the observed soft X ray and spectroscopic line emission. From a different experimental viewpoint [18], an analysis of the electron energy power balance has been conducted in JET ohmic discharges at times before and after the sawtooth crash. The result also yields very low values for the central χ_e , of the order of 0.12 m^2/s.

The order of magnitude difference in the value for the diffusion coefficient χ_e calls for discussion. There are two different ways in measuring χ_e : one is global, deduced from the measurement of the overall confinement time, and the other dynamical deduced up to now, from the observation of the heat pulse propagation. The latter, as opposed to the global value, is derived from the quiescent phase of the sawtooth and takes account of the temperature gradient effects [5,19]. The value deduced for χ_e is related to the gradient zone of the profile, and is averaged over a few sawteeth using the boxcar technique [5].

The estimation of χ_e obtained by the modulation technique, as in the case of heat pulse propagation, applies only to the quiescent sawtooth phase. The acquisition time being long, the source of perturbation (i.e. the sawtooth crash) is actually replaced by the modulated RF power. The difference in the two methods lies in the location of the measurement, which is

made on opposite side of the inversion radius. Although the two methods are mutually exclusive during the same shot, measurements performed on similar sawtoothing discharges, show that the dynamically measured χ_e is lower inside than outside the inversion radius by approximately an order of magnitude.

Eventually, those results have received some theoretical support [20] in a model where the question of the toroidal electric field profile effect on χ_e is addressed. The sawtoothing discharge is described by a set of two coupled equations for $T_e(r,t)$ and $B_\theta(r,t)$. In the case where the profile is taken non uniform, the resulting χ_e deduced from the power balance is considerably lower (as much as one order of magnitude) inside the q=1 surface than when the profile is kept constant, supporting our observation.

Finally, it should be noted that RF modulation experiments conducted in monster sawtooth regimes have shown a central diffusivity χ_e in the range 2 - 4 m^2/s [21]. However [22], in such regime the electron temperature gradient is large (typically 10 keV/m) and remains large during the all modulation experiment, contrarily to the case presented here. A detailed account of monster modulation experiments will be presented separately.

VI. CONCLUSIONS.

The ICRF modulation experiment in JET has demonstrated to be a powerful tool to investigate both the RF power deposition profile and the diffusion in the central zone of the plasma discharge. However, in cases of indirect heating the integration provided by the minority has an adverse effect and requires more modulation power. More damaging is the correlation with the sawtooth crashes, but this problem has been overcome in experiments with monster sawtooth.

In D(He^3) where direct heating is measurable, the power deposition profile appears localized and the transport of power by conduction can be observed. Modulation experiments allows for an estimation of χ_e without assumption on the amount of power deposited, which is a favorable advantage. This technique should become a standard χ_e diagnostic using either ICRF in cases of mode conversion or strong direct Landau damping, or ECRH when high power, long pulse gyrotrons will become available.

Although it was a primary goal of RF modulation experiments, a detailed comparison between experimental observations and theoretical predictions is difficult for the heating schemes reported here. It is only when there is direct RF heating of electrons through mode conversion that the shape and amplitude of the power deposition may be accessed experimentally. This situation is also the most difficult to describe numerically. As there is no large differences in the location of the cyclotron and mode conversion layer and as they are both

located close to the plasma center, the experimental power deposition profile is always observed around $\omega = \omega_{ci}$ and its narrowness is in general agreement with what is expected for the JET geometry.

Acknowledgements: authors are grateful to Drs G. Bracco, R. Gianella and J.H. Hamnén for fruitful discussions and to the machine operation team, in particular the ECE group.

REFERENCES.

[1] Callen, J.D., Christiansen, J.P., Cordey, J.G, Thomas, P.R., Thomsen, K., Nuclear Fusion 27 (1987) 1857.

[2] Hammett, G.W., 'Fast Ion Studies of Ion Cyclotron Heating in the PLT Tokamak', Princeton Ph.D. Thesis (1986).

[3] Kaye, A.S., in Fusion Engineering (Proc. 11th Symp. Austin, TX, 1985), Vol.2,IEEE, New York (1986) 1204.

[4] Gambier, D.J., Bartlett, D.V., Bures, M., et al., in Cont. Fusion and Plasma Physics 12th European Conf., E.P.S. Budapest (1985). European Physical Society, Vol.9F, pt.II (1985) 152.

[5] Tubbing, B.J.D., Lopes Cardozo, N.J., Van der Wiel, N.J., Nuclear Fusion 27 (1987) 1843.

[6] Costley, A.E., Baker, E.A.M, Brusati, M. et al., in Cont. Fusion and Plasma Physics, 12th European Conf., E.P.S. Budapest (1985), European Physical Society, Vol. 9F, pt. I (1985) 227.

[7] Tubbing, B.J.D., Piekaar, H.W., Barbian E.P., Ned. Tijdschrift voor Natuurkunde B52 (1986) 42.

[8] Daly, E.J. et al., Plasma Physics and Cont. Fusion 27 (1985) 761.

[9] Smith, D.E., Powers, E.J., Caldwell, G.S., IEEE Trans. on Plasma Science,Vol. PS-2, (1974) 261.

[10] Barbato, E., Giannella, R., Physics Letters 110A, 6 (1985) 309.

[11] Giannella, R., Zanza, V., Barbato, E., Bracco, G., Corti, S., Gambier, D.J., Nuclear Fusion 28 (1988) 193.

[12] Stix, T.H., Nuclear Fusion 15 (1975) 737.

[13] Evrard, M.P.,in Cont. Fusion and Plasma Physics, 14th European Conf., E.P.S. Madrid (1987), European Physical Society, Vol. 11D, pt. III (1987) 809.

[14] Book, D.L., "NRL Plasma Formulary", Naval Research Lab., Washington DC.

[15] White, R.B., Rutherford, P.H., Colestock, P.L., Bussac, M.N., in Cont. Fusion and Plasma Physics, 15th European Conf., E.P.S. Dubrovnik (1988), European Physical Society, Vol. 12B, pt. I (1988) 413.

[16] Edery, D., Picq, H., Samain, A., Gambier, D.J., Rep. CEN Cadarache, DRFC/CAD, EUR-CEA-FC-1334 (1987).

[17] Compant La Fontaine, A., Dubois, M.A., Pecquet, A.L., Boyd, D., Cavallo, A., Cohen, S. et al., Plasma Physics and Controlled Fusion 27, 3 (1985) 229.

[18] Stringer, T.E., Cordey, J.G., JET private communication.

[19] Gentle, K.W., Phys. Fluids 31, 5 (1988) 1105.

[20] Alladio, F., Vlad, G., Phys. Fluids 31, 3 (1988) 602.

[21] Tibone, F., Evrard, M.P., Bhatnagar, V., et al., in Proc. 15th Eur. Conf. on Controlled Fusion and Plasma Heating, Dubrovnik, Vol. 12B Pt. II (1988) 709.

[22] Rebut, P.H, Brusati, M., Hugon, M., Lallia, P., in Plasma Physics and controlled Nuclear Fusion Research (Proc. 11th Int. Conf., Kyoto, 1986) Vol 2 (1987) 187.

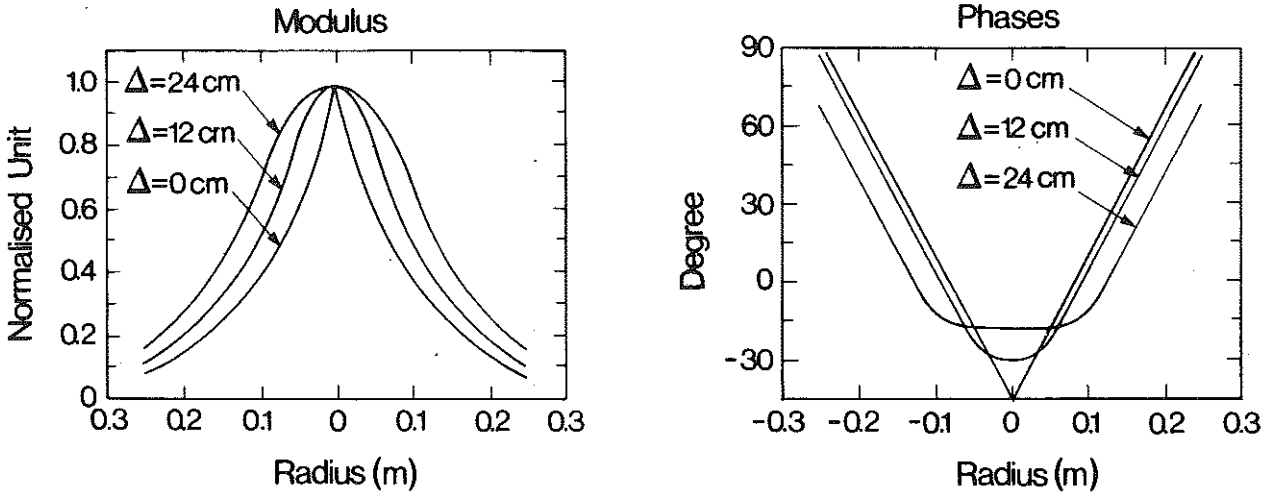

Fig. 1(a) Evolution with radius of the modulus and phase of the electron energy response to a sinusoidal RF power signal. Modulation frequency 5 Hz, square power deposition profile of extension $\Delta(\Delta = 0, 12, 24\,\text{cm})$, amplitude normalized to $P\Delta$, and $\chi_e = 0.25\,\text{m}^2/\text{s}$.

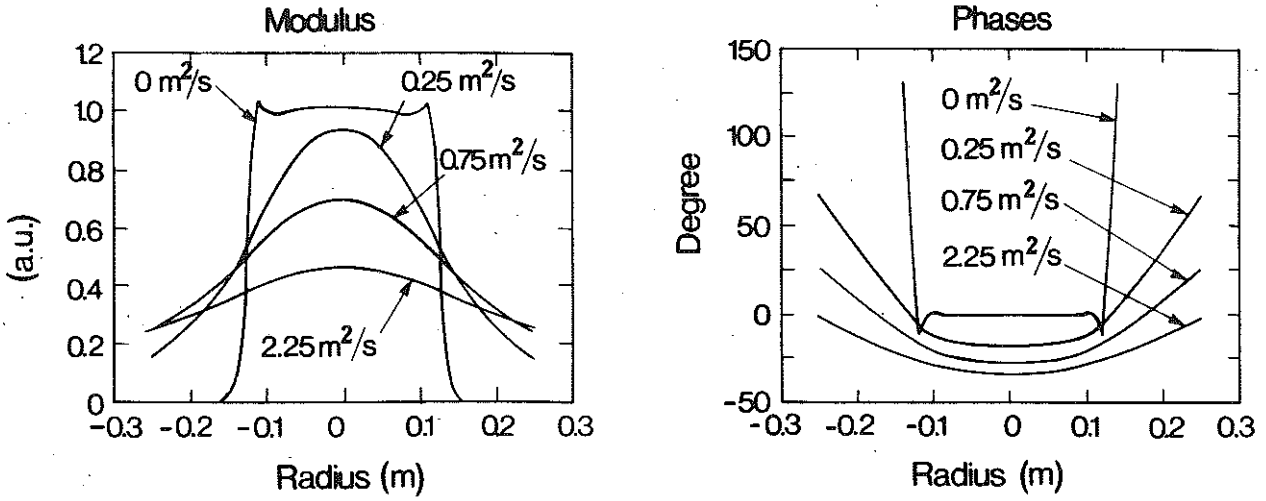

Fig. 1(b) Evolution with radius of the modulus and phase of the electron energy response to a sinusoidal RF power signal. Modulation frequency 5 Hz, square power deposition profile of extension $\Delta(\Delta = 12.5\,\text{cm})$ and $\chi_e = 0.001, 0.25, 0.75, 2.25\,\text{m}^2/\text{s}$.

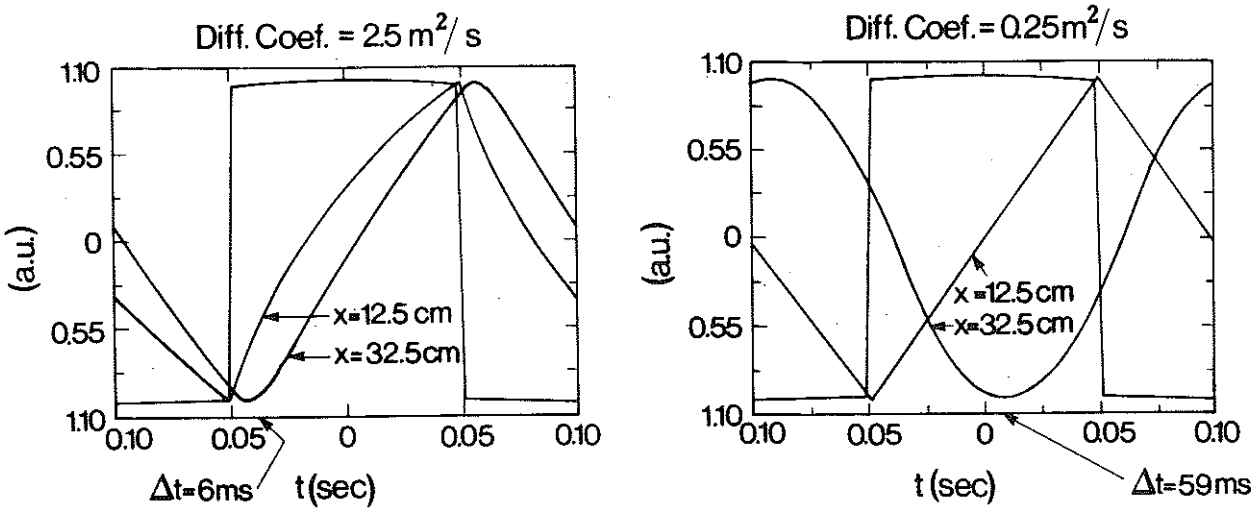

Fig. 2 Response evolution of the electron temperature to a square wave modulation ($\nu = 5$ Hz), at two locations ($x = \Delta = 12.5$ cm and $x = \Delta + 20$ cm and for two χ_e values ($\chi_e = 0.25$ and $2.5\,m^2/s$).

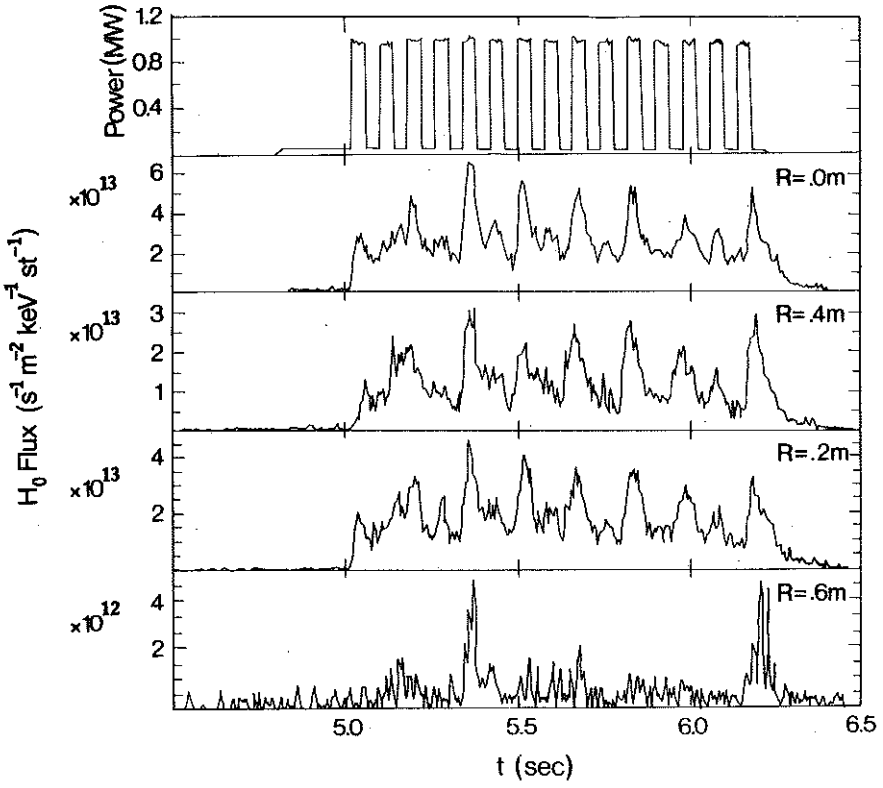

Fig. 3 Neutral flux signal at different observation angles during ICRF modulation in D(H) plasma.

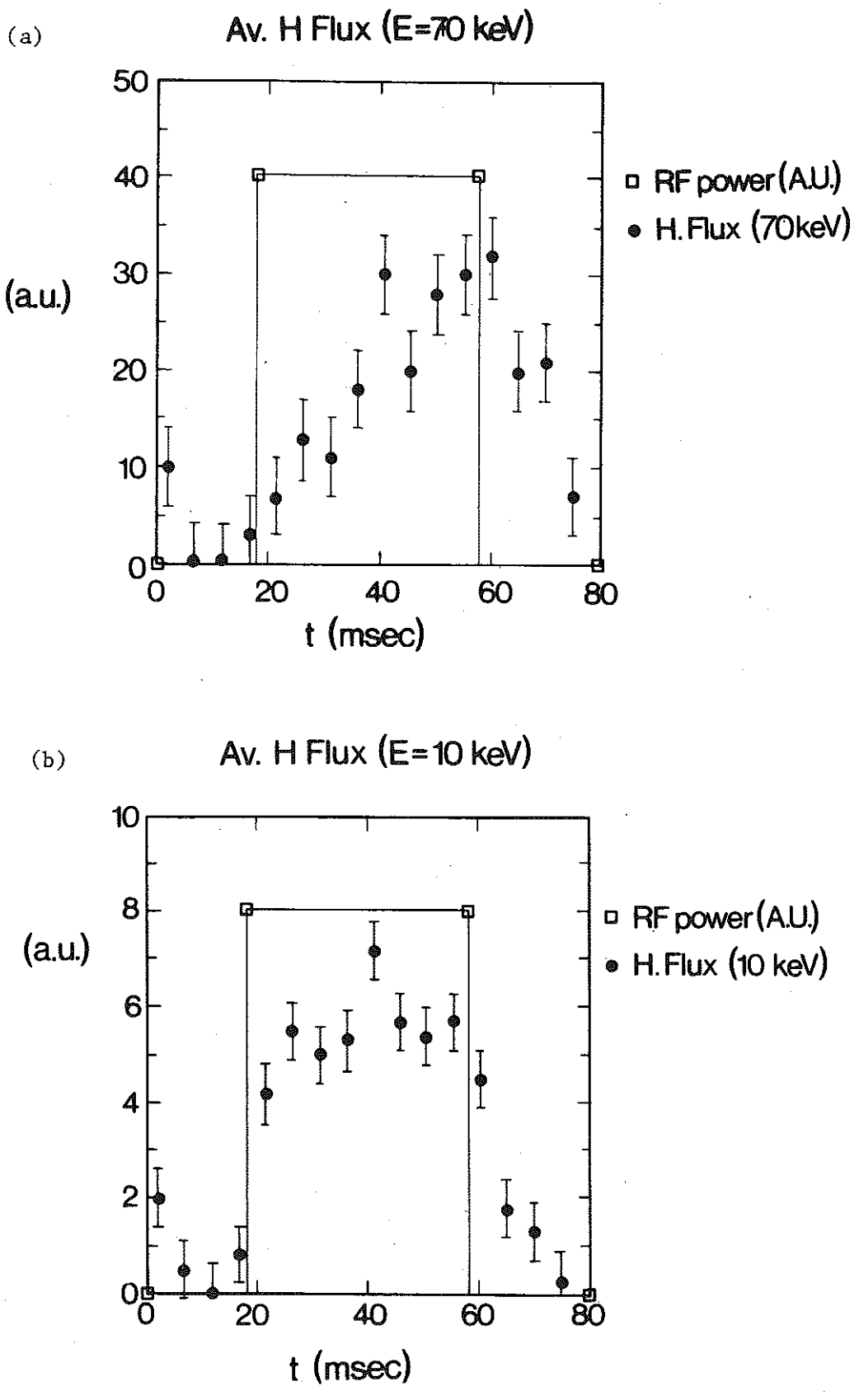

Fig. 4 Averaged response in time to the modulation pulse for the central channel (R=.0m) and for two energies ((−a) E=10keV and (−b) E=70keV).

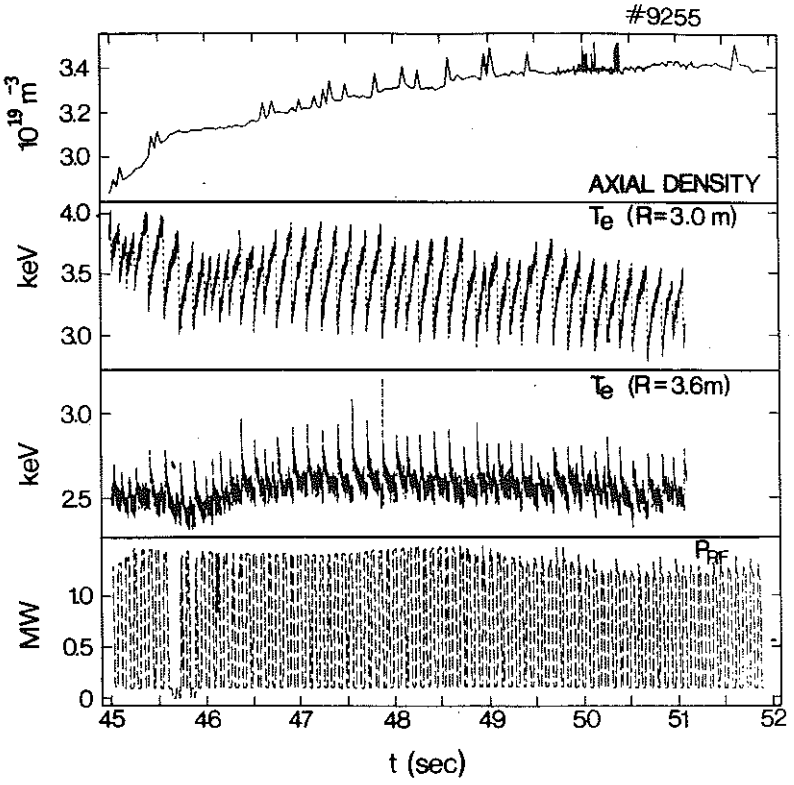

Fig. 5 Evolution of various parameters during ICRF modulation in D(H) plasmas: (1) central density, (2) central electron temperature, (3) electron temperature at mid radius, (4) deuterium temperature, (5) modulated RF power.

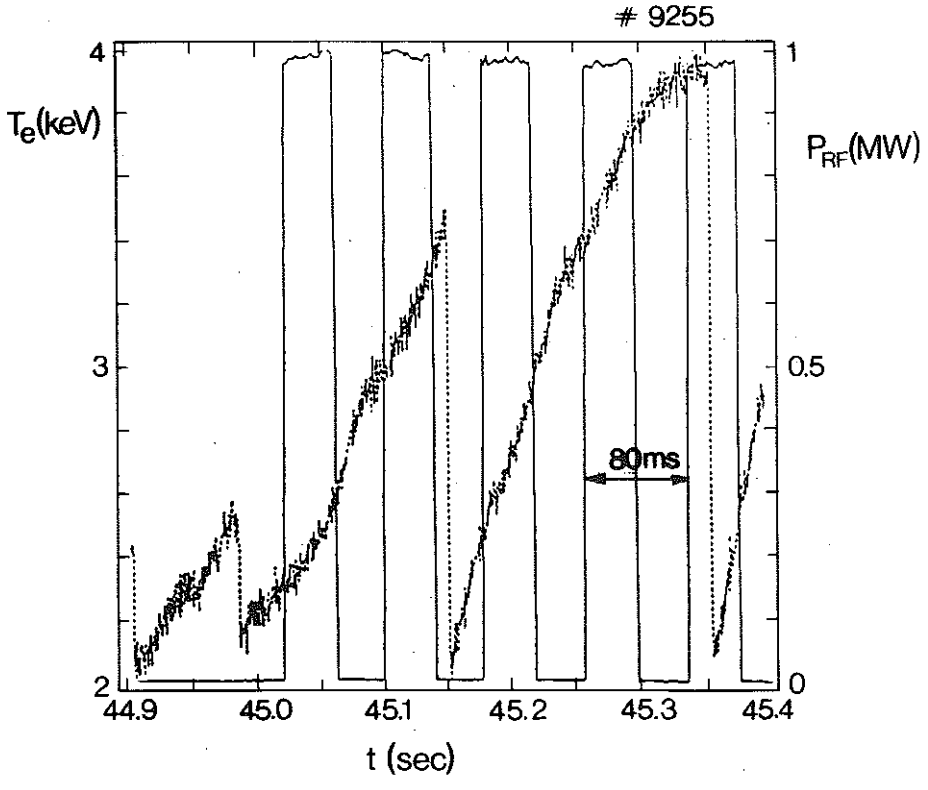

Fig. 6 Evolution of the central electron temperature at the onset of the ICRF modulated pulse.

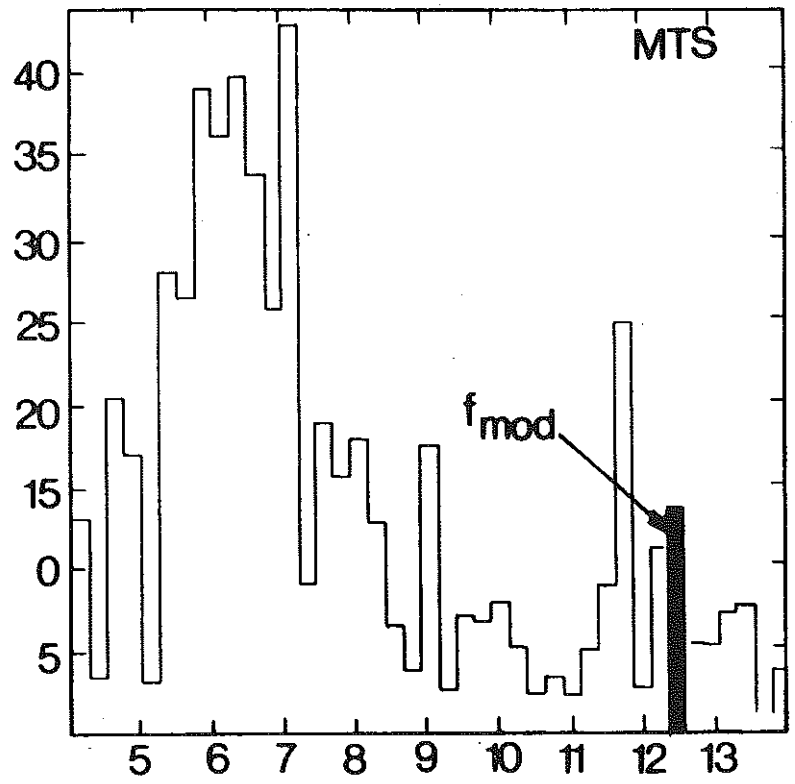

Fig. 7(a) Amplitude Fourier spectrum for the central modulated temperature signal (MTS).

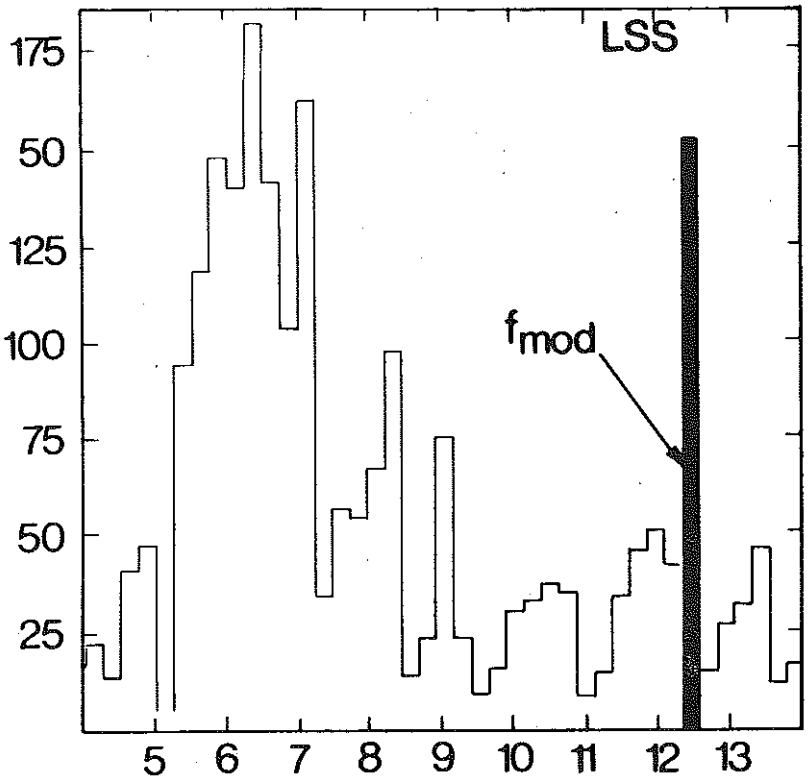

Fig. 7(b) Amplitude Fourier spectrum for the central linearized sawtooth crash signal (LSS).

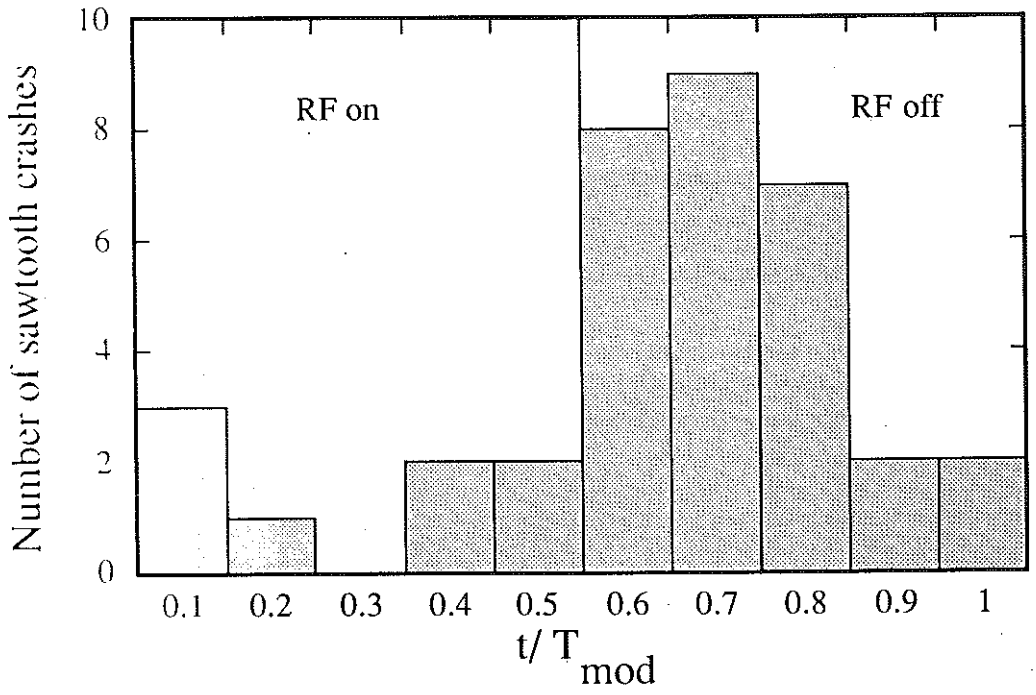

Fig. 8 Histogram of the number of sawtooth crashes, occurring during the RF on and off phase, plotted as a function of the modulation period (D(H) plasma P_{Rf}=1 MW peak to peak).

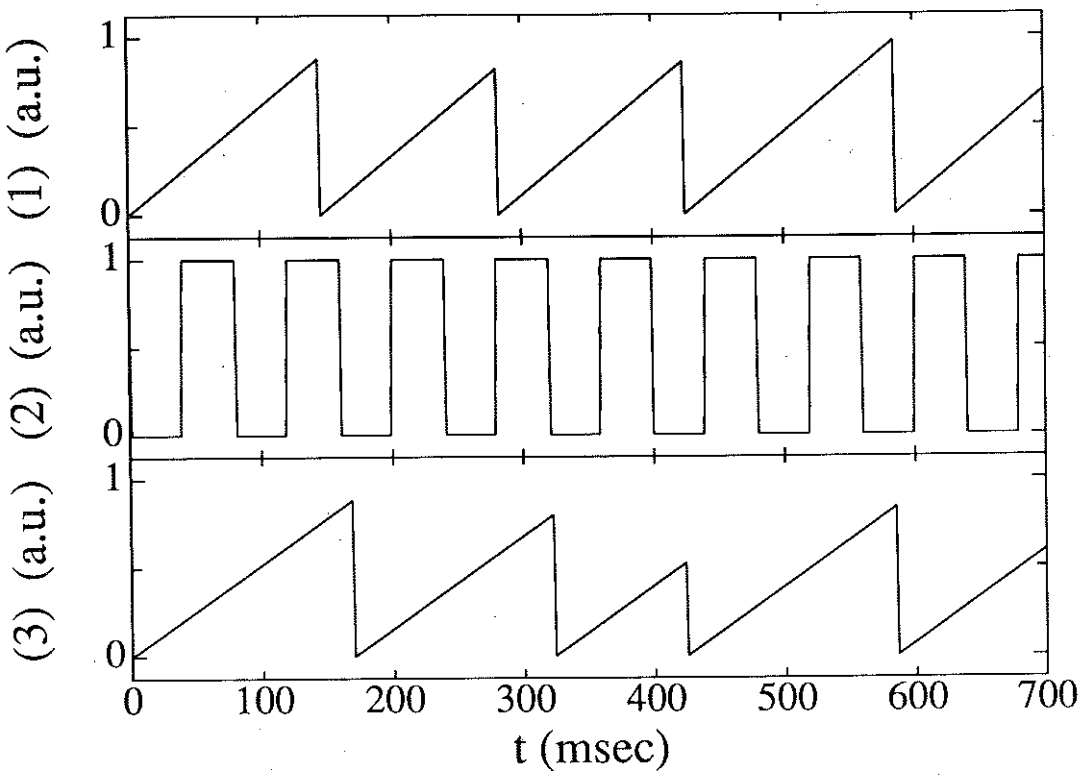

Fig. 9 Simulation of the sawtooth crash correlation vs. time: (1) sawtooth not correlated, (2) RF modulated signal, (3) sawtooth crashes correlated.

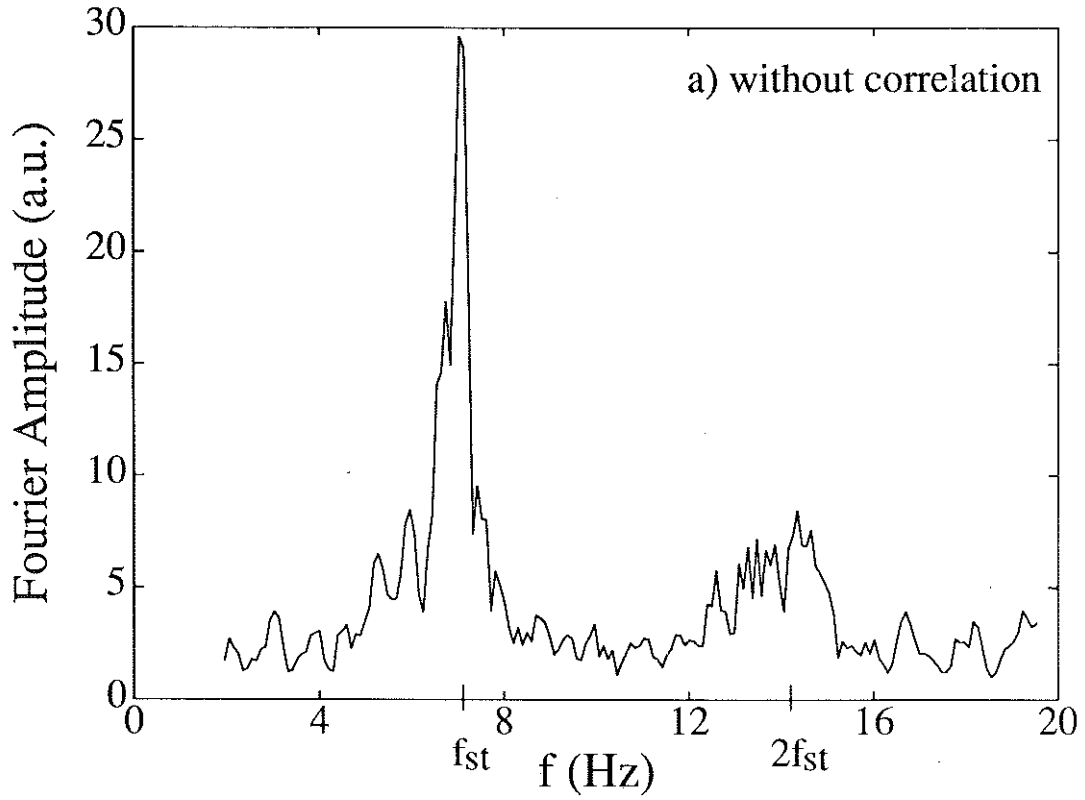

Fig. 10(a) Non correlated sawtooth Fourier spectrum where f_{st} stands for the quasi sawtooth frequency.

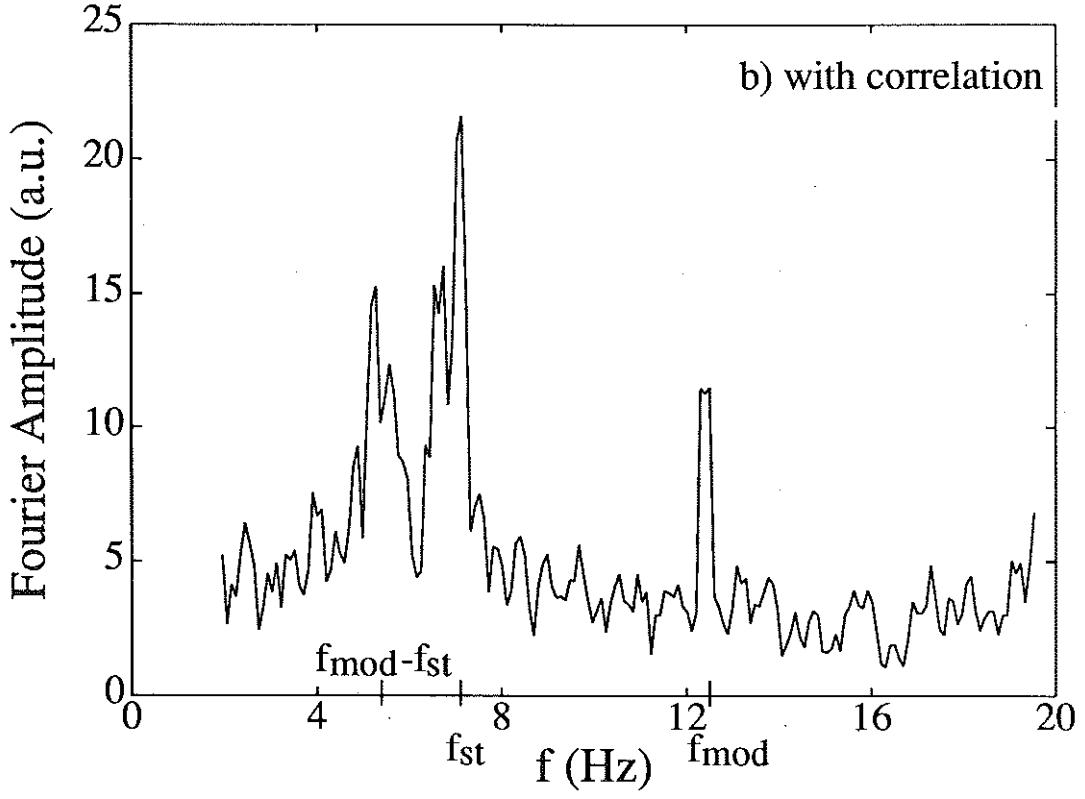

Fig. 10(b) Correlated sawtooth Fourier spectrum.

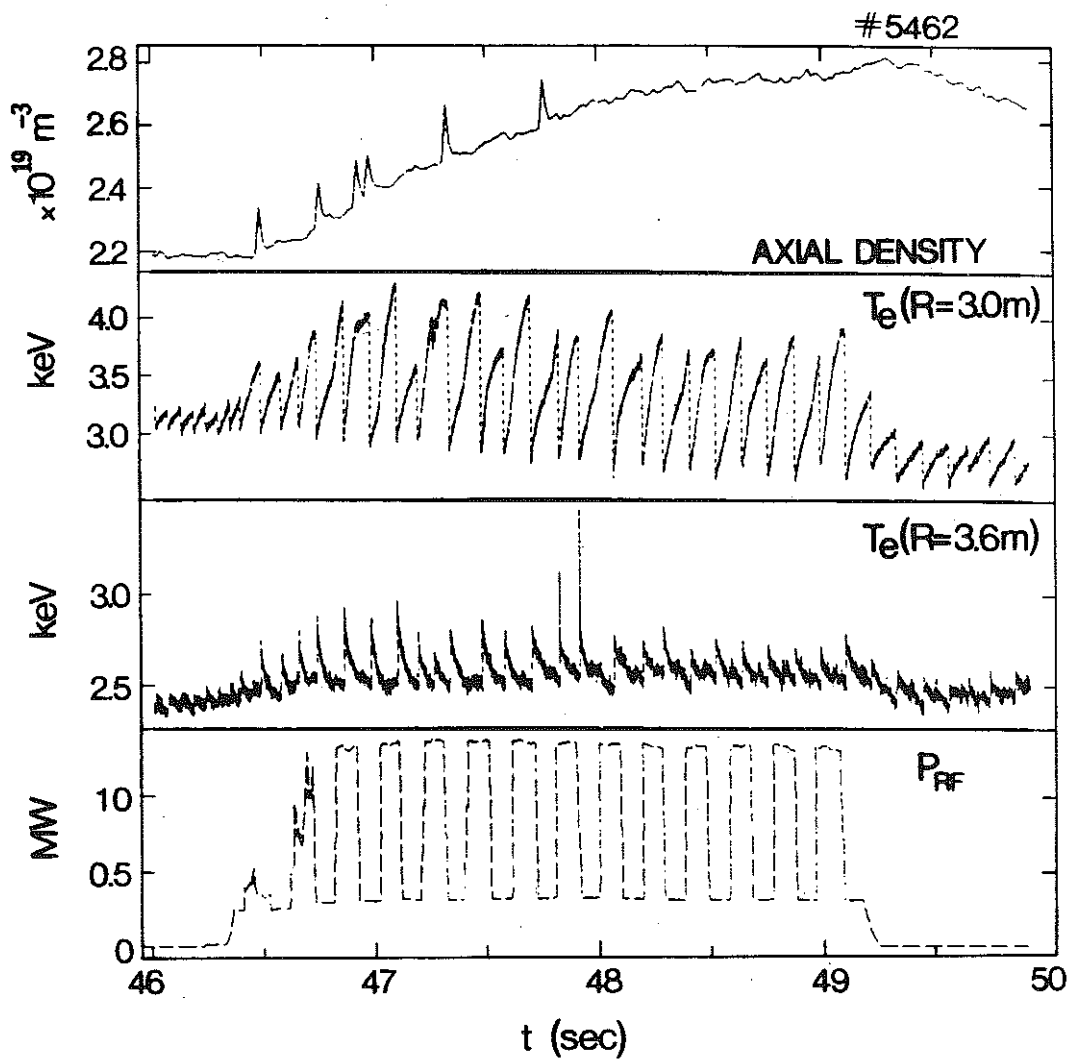

Fig. 11 Evolution of various parameters during ICRF modulation in D(He^3) plasmas: (1) central electron density, (2) Deuterons temperature, (3) central electron temperature, (4) modulated RF power.

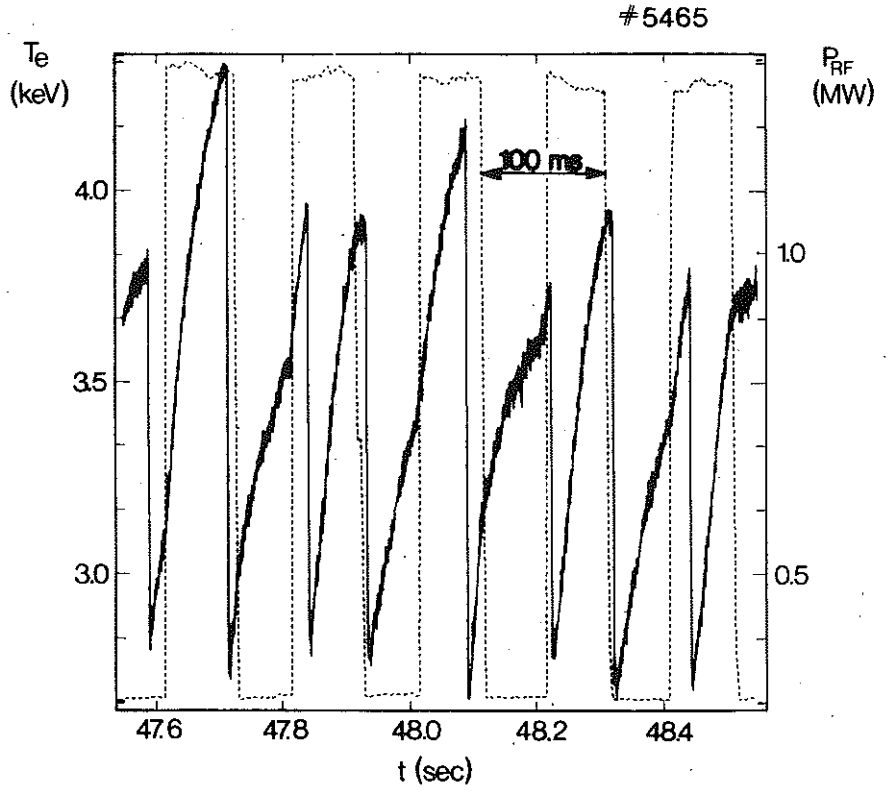

Fig. 12(a) Evolution of the central $T_e(t)$ during the RF pulse.

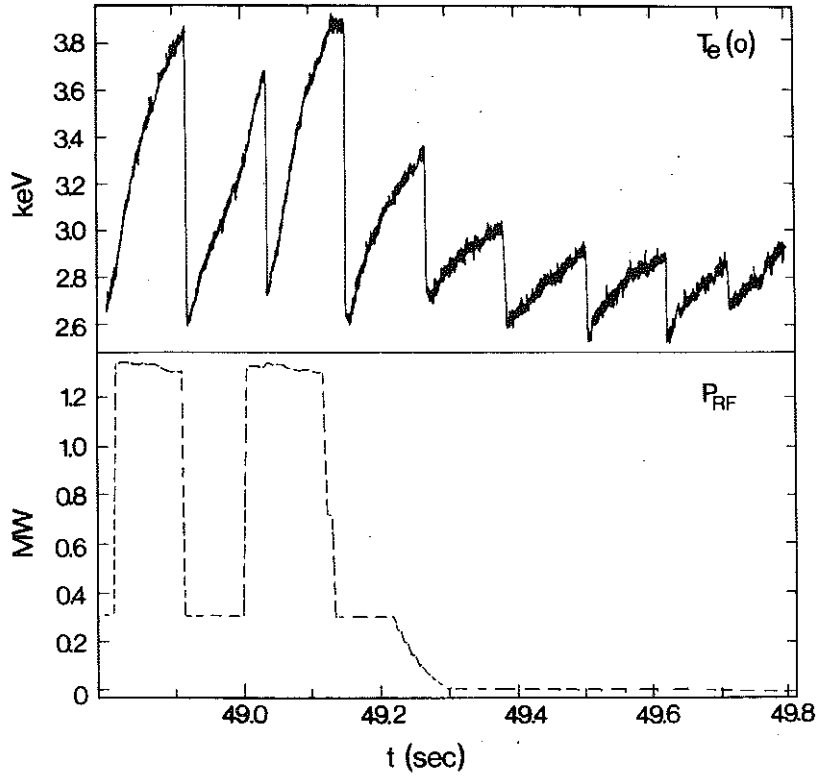

Fig. 12(b) Evolution of the central $T_e(t)$ at the end of the RF pulse.

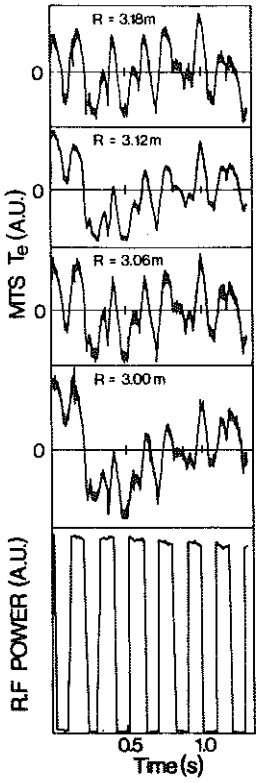

Fig. 13 Evolution of the modulated $T_e(t)$ during the RF pulse.

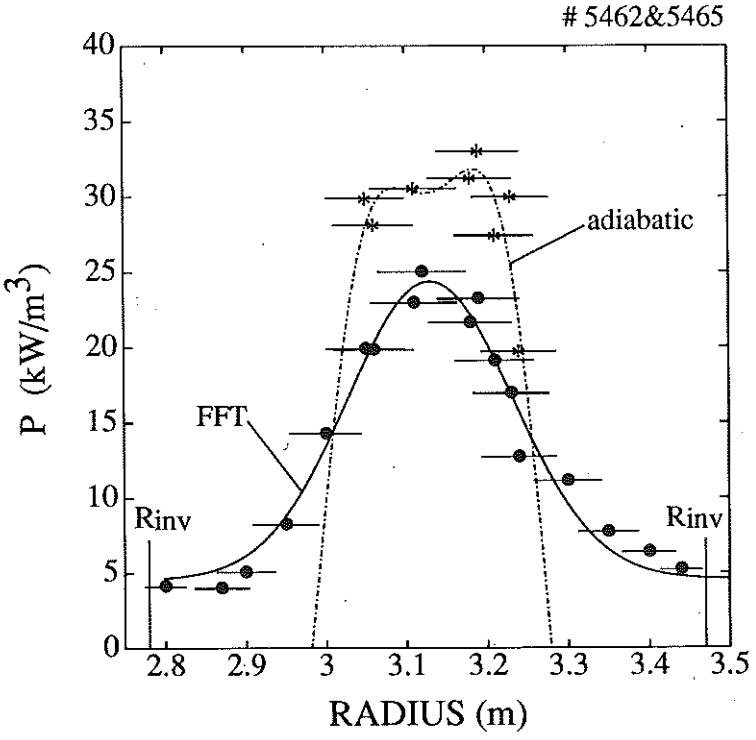

Fig. 14 Amplitude Fourier spectrum $\bar{W}_{e\tilde{\omega}}(r)$ of the electron energy vs. radius at the modulation frequency (5 Hz), and the adiabatic amplitude $\langle We(r) \rangle$ response averaged over the number of onsets and offsets of the RF power.

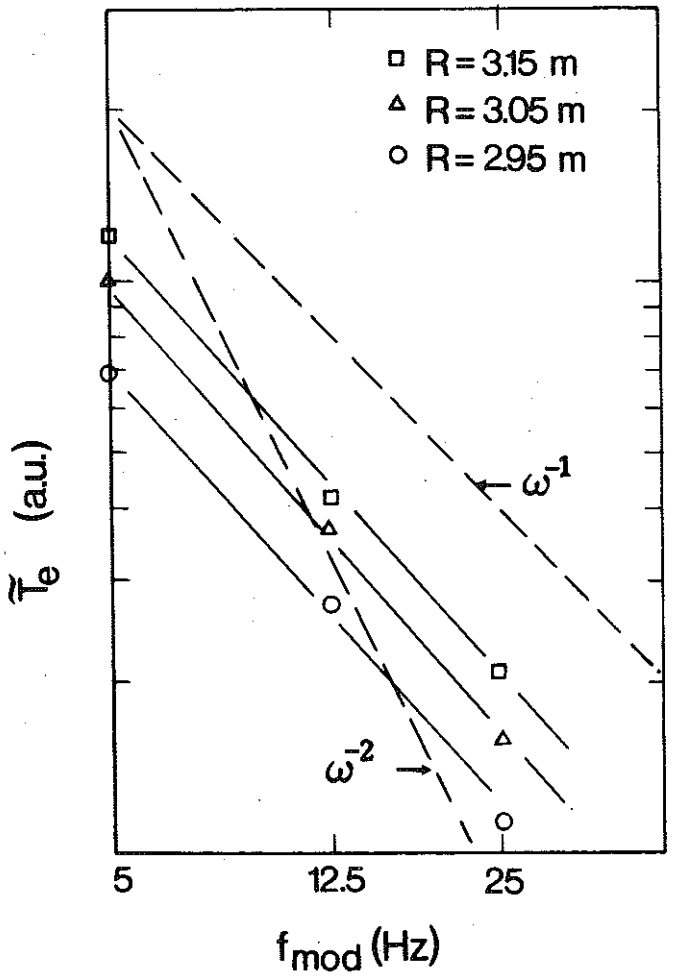

Fig. 15 Fourier amplitude of the central $\bar{T}_e(\tilde{\omega})$ for different modulation frequencies (5, 12.5, 25 Hz), showing the $1/\tilde{\omega}$ evolution.

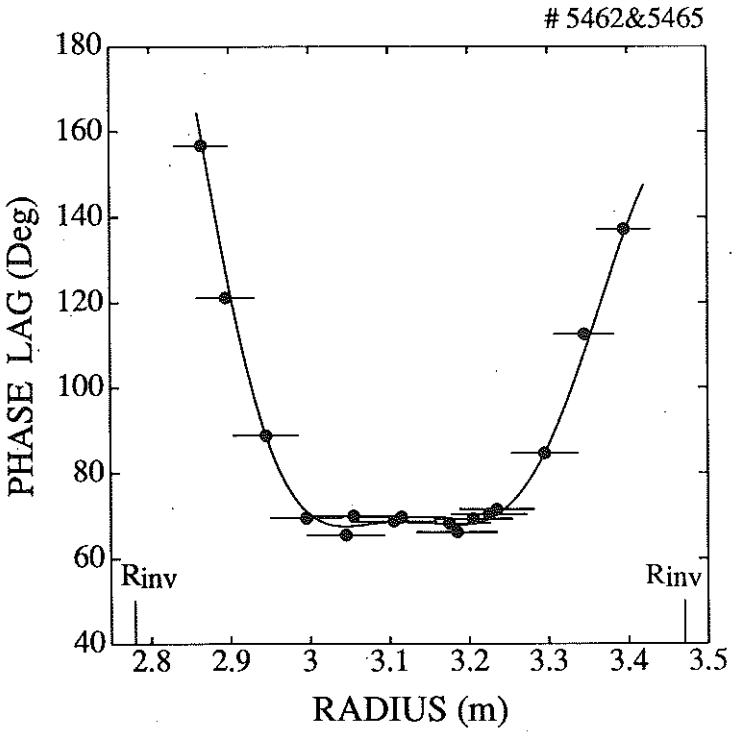

Fig. 16(a) Phase Fourier spectrum of $\tilde{W}_{e\omega}(r)$, from which a χ_e of $0.24 \pm 0.05\,m^2/s$ is deduced.

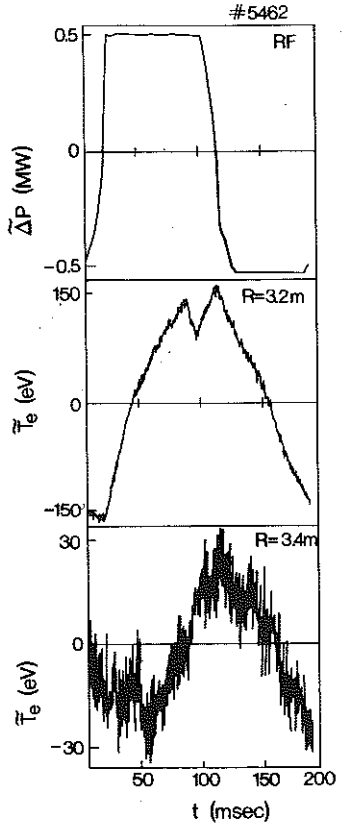

Fig. 16(b) Averaged response to the square modulated pulse for the MTS at different radii ($R = 3.30$ and $3.40\,m$). The result may be simulated by $\chi_e \approx 0.27 \pm 0.04\,m^2/s$.